PAPER

Inverse vulcanization of trimethoxyvinylsilane particles†

Alexander P. Grimm, [a] Johannes M. Scheiger,[b] Peter W. Roesky [c] and Patrick Théato ★[a,d]

Elemental sulfur, a highly abundant waste product from natural gas and oil refining, can be used to create polymeric materials when reacted with unsaturated organic comonomers at elevated temperatures. Herein, we report on the inverse vulcanization of trimethoxyvinylsilane (TMVS) particles to obtain sulfur coated TMVS-sulfur (TMVS-S) particles with a sulfur content of 18.85 wt%. TMVS-S particles exhibit a high surface-to-volume ratio, insolubility, and can further be functionalized with *N*-vinylimidazole (*N*VIA) to incorporate N-donor ligands, known for copper(II) complexation. Adsorption experiments with aqueous solutions of mercury(II) and copper(II) ions revealed very good distribution coefficients of TMVS-S-*N*VIA particles for mercury and copper remediation, showcasing possibilities arising from combining inorganic siloxane and sulfur polymers towards novel adsorbent materials derived from abundant and commercially available compounds.

Introduction

The desulfuration of natural oil and gas has increased the global annual production of elemental sulfur to over 70 million tons caused by the great demand for fossil fuels of our modern civilization. However, the need for elemental sulfur as a resource for industrial production of sulfuric acid, fertilizers, vulcanized rubbers, and cosmetics is greatly outweighed by its production, resulting in a phenomenon called the 'excess sulfur problem'.[1] The abundance of cheap elemental sulfur on the megaton scale gave rise to its application as an alternative feedstock for polymeric materials. In 2013, Pyun *et al.* introduced the concept of inverse vulcanization, a polymerization method capable of producing stable copolymers with sulfur contents over 90 wt%. Upon exceeding the temperature of the melting point of S_8, the covalent bonds of cyclic S_8 molecules are homolytically cleaved resulting in the formation of sulfur diradicals that polymerize to form polymeric sulfur.[2] The principle of inverse vulcanization relies on the addition of unsaturated olefins, so-called cross-linkers, to the reaction mixture that inhibit the depolymerization of sulfur chains and stabilize the obtained material.[3] In 2019, Hasell *et al.* introduced the concept of catalyzed inverse vulcanization which greatly increased the range of vulcanizable organic compounds including vinylsilanes.[2] By addition of a catalyst, *e.g.* zinc diethyldithiocarbamate (Zn(DTC)$_2$), the reaction temperature during inverse vulcanization may be lowered considerably while reducing the formation of toxic H_2S as a byproduct.[4] Inverse vulcanized polymers have shown to be cheap and accessible materials for applications such as infrared optics,[5–10] antibacterial surfaces,[11,12] healable materials,[13–15] fertilizers,[16] thermal insulators,[17] and Li–S battery cathodes.[18–23] Importantly, inverse vulcanized materials have been demonstrated to effectively remove highly toxic mercury ions from aqueous solutions in the past years.[24–29] However, increasing the uptake capacity of inverse vulcanized materials towards other potentially hazardous heavy metals, besides mercury, remains challenging as it typically requires either the use of comonomers that are not available on a large scale[30,31] or microporous design.[31–34] We previously reported the successful inverse vulcanization of unsaturated hydrolysable alkoxy silanes, capable to undergo polycondensation, resulting in the formation of stable siloxane bound polymers with high sulfur content.[35] Combination of inverse vulcanization with silane chemistry has turned out to be a promising technique to introduce a unprecedented amount of control over macroscopic properties of polymeric materials synthesized *via* inverse vulcanization.[36] In 1968, the controlled synthesis of spherical silica particles has been described for the first time.[37] Ever since, functionalized silica particles have

ᵃInstitute for Chemical Technology and Polymer Chemistry (ITCP), Karlsruhe Institute of Technology (KIT), Engesserstr. 18, 76131 Karlsruhe, Germany. E-mail: patrick.theato@kit.edu

ᵇInstitute of Biological and Chemical Systems – Functional Molecular Systems (IBCS-FMS), Karlsruhe Institute of Technology (KIT), Herrmann-von-Helmholtz-Platz 1, 76344 Eggenstein-Leopoldshafen, Germany

ᶜInstitute of Inorganic Chemistry (AOC), Karlsruhe Institute of Technology (KIT), Engesserstr. 15, 76131 Karlsruhe, Germany

ᵈInstitute for Biological Interfaces III (IBG-3), Karlsruhe Institute of Technology (KIT), Hermann-von-Helmholtz-Platz 1, 76344 Eggenstein-Leopoldshafen, Germany

become available in large quantities due to their application in the fields of nanotechnology,[38] biological drug-delivery,[39] personal care products,[40] pesticides,[41] and adsorption materials.[42]

In the present study, we report on the inverse vulcanization of vinylated silica particles utilizing abundant elemental sulfur and affordable commercially available compounds in a straightforward reaction technique. Spherical vinylated microscale particles can be obtained by a modified Stöber synthesis and can be coated efficiently by inverse vulcanization when $Zn(DTC)_2$ is used as a catalyst. Due to a high surface-to-volume ratio of the microscale particles, the synthesized trimethoxyvinylsilane-sulfur (TMVS-S) particles are hypothesized to represent an efficient adsorbent material for mercury removal from aqueous solutions.[33] The presented system is further improved to also efficiently bind copper(II) ions from aqueous solutions up to 10 ppm by introducing N-vinylimidazole (NVIA) into the sulfur coating of the particles (TMVS-S-NVIA particles). Synthesized materials were characterized with bulk methods such as EA and TGA, as well as surface sensitive analytic methods such as EDX, ATR FT-IR, and SEM. The adsorption performance of sulfur coated TMVS particles, as well as post-modified TMVS-S-NVIA particles is determined by cold-vapor AAS and ICP-AES.

Experimental

Materials

Ammonia solution (Roth, 25%), carbon disulfide (Acros Organics, 99.5%), copper(II) chloride (Sigma Aldrich, anhydrous), ethanol (Thermo Scientific, 99.5% anhydrous), mercury(II) chloride (Fisher, anhydrous), sulfur (Alfa Aesar, 99.5%), tetrahydrofuran (AnalaR NORMAPUR), trimethoxyvinylsilane (TCI, 98%), 1-vinylimidazole (Sigma Aldrich, 99%), and zinc diethyldithiocarbamate (Sigma Aldrich, 97%) were used as received.

Characterization

ATR FT-IR spectra were recorded on a Bruker Vertex 80 from 500 to 4000 cm^{-1} at 25 °C with a resolution of 2 cm^{-1}.

Elemental analysis was performed via thermal combustion with an Elementar Vario Microtube device from Elementar at a temperature of about 1100 °C.

Thermal gravimetric analysis was carried out using a TGA 5500 from TA Instruments at a heating rate of 10.0 K min^{-1} under nitrogen atmosphere up to 1000 °C. Typically, about 5 mg material were weighed on a platinum pan prior to the measurements.

DSC measurements were conducted using a TA DSC 2500 with a heat rate of 10 K min^{-1} between 25 °C and 150 °C in TA Tzero sample holders.

All analyzed particles were investigated with a LEO 1530 scanning electron microscope from Leica with an accelerating voltage of 5–10 kV. For SEM analysis the samples were sputtered with a thin layer of carbon. For EDX spectroscopy a NORAN System SIX from Thermo Scientific was used.

The specific surface areas of the particles were determined by nitrogen physisorption vie the Brunauer–Emmett–Teller (BET) method. The analysis was performed with a Rubotherm BELSORP-mini II. All particles were pretreated in vacuum at 100 °C for 2 h prior to N_2 dosing.

ICP-AES measurements were determined using an ICP-AES 5100 SVDV, type G8010A from Agilent equipped with an SPS3 648480A autosampler. Samples were filtered through 0.45 μm pores and acidified with 100 μL 65% HNO_3 per 10 mL sample volume.

Cold-vapor AAS measurements were performed using a QuickTrace M-7600 from Teledyne Leeman Labs. Bromination reagent was added prior to measurements.

Synthesis of vinylated silica particles (TMVS particles)

Vinylated silica particles were synthesized based on a previously published method.[43] In a 250 mL round bottom flask equipped with a magnetic stirring bar ethanol (50 mL, 39.5 g) and an NH_4OH solution (25% w/v, 20 mL, 18.9 g) were added. Trimethoxyvinylsilane (5 mL, 4.5 g, 23.6 mmol) was added dropwise under vigorous stirring and the solution was kept at room temperature for 4 hours. Cloudiness was observed after 15 min. The reaction mixture was filtered and washed with DI water (3 × 20 mL) and ethanol (2 × 20 mL). Drying in a vacuum oven at 40 °C for 18 hours yielded 2.67 g vinylated TMVS particles in the form of a colorless powder.

ATR-FT-IR: ν/cm^{-1} = 3060, 2957, 1602, 1408, 1276, 1115, 1004, 1037, 964, 757.

EDX: keV = 0.27 (C K_α), 0.52 (O K_α), 1.72 (Si K_α).

Inverse vulcanization of vinylated silica particles (TMVS-S particles)

In a 10 mL crimping vial equipped with a magnetic stirring bar 1.0 g of previously prepared vinylated TMVS particles were placed. Elemental sulfur (5 g, 19.5 mmol) and zinc diethyldithiocarbamate (100 mg, 0.276 mmol) were added and the content was thoroughly mixed. The vial was sealed and placed in a temperature-controlled heating block at 150 °C for 2 hours. The reaction mixture was filtered and thoroughly washed with CS_2 (3 × 50 mL), THF (3 × 50 mL), and ethanol (2 × 50 mL) to remove any excess of sulfur. Drying in a vacuum oven at 40 °C for 18 hours yielded 1.30 g sulfurated TMVS-S particles in the form of a yellow powder.

ATR-FT-IR: ν/cm^{-1} = 3060, 2957, 1602, 1408, 1276, 1115, 1004, 1037, 964, 757.

EDX: keV = 0.27 (C K_α), 0.52 (O K_α), 1.02 (Zn K_α), 1.72 (Si K_α), 2.31 (S K_α), 2.46 (S K_β).

Modification of inverse vulcanized vinylated silica particles via dynamic covalent polymerization (TMVS-S-NVIA particles)

Sulfurated TMVS-S particles (200 mg) were placed in a 10 mL crimping vial equipped with a magnetic stirring bar. Zinc diethyldithiocarbamate (10 mg, 27.6 μmol) and N-vinylimidazole (1.0 g, 10.6 mmol) were added. As result the powder was fully submerged. The vial was sealed and placed in a temperature-controlled heating block at 150 °C for 2 hours. The reaction

mixture was filtered and washed with THF (2 × 20 mL) and ethanol (2 × 20 mL). Drying in a vacuum oven at 40 °C for 18 hours yielded 170 mg modified inverse vulcanized TMVS-S-*N*VIA particles in the form of a brown powder.

ATR-FT-IR: ν/cm^{-1} = 3060, 2957, 1647, 1602, 1500, 1408, 1276, 1228, 1109, 1032, 1004, 964, 882, 757, 654.

EDX: keV = 0.27 (C K_{α}), 0.39 (N K_{α}), 0.52 (O K_{α}), 1.02 (Zn K_{α}), 1.72 (Si K_{α}), 2.31 (S K_{α}), 2.46 (S K_{β}).

Adsorption of mercury(II)- and copper(II) ions from aqueous solution by modified inverse vulcanized silica particles

Modified inverse vulcanized TMVS-S-*N*VIA particles (200 mg) were placed in a 250 mL round bottom flask equipped with a magnetic stirring bar. A solution containing mercury(II) and copper(II) chloride (concentrations see below) in DI water (100 mL) were added and the mixture was stirred at room temperature for 24 hours. The reaction mixture was filtered, and the resulting mercury(II) and copper(II) concentrations were determined by cold-vapor AAS and ICP-OES, respectively. Four adsorption reactions were conducted with initial concentrations of both mercury(II) and copper(II) ions being 1, 10, 100, and 1000 mg L^{-1}.

Results and discussion

In the present study, the inverse vulcanization of vinyl functionalized silica particles was carried out for the first time (Scheme 1). First, the synthesis of vinylated silica particles (TMVS particles) was carried out by utilizing a modified Stöber synthesis by reacting trimethoxyvinylsilane (TMVS) in ethanol with aqueous ammonia solution as reported previously.[43] TMVS particles were isolated *via* filtration and washed with DI water and ethanol to stop particle growth and remove unreacted monomer. ATR FT-IR analysis of TMVS particles confirmed the formation of highly cross-linked Si–O–Si networks by the disappearance of the Si–OMe stretch vibration at 1078 cm^{-1} and the formation of a very strong and broad characteristic vibrational band in the region of 1120 to 1000 cm^{-1} (Fig. S1 and S2†).[44] Absorbance bands at 1602, 1408, 964, and 757 cm^{-1} could be attributed to the respective C=C$_{\text{stretch}}$, C–H$_{\text{bend}}$, and C–H$_{\text{wag}}$ vibrations in C=C–H of vinyl groups in the synthesized particles. Due to the hydrophobic nature of the vinyl groups on the surface of the TMVS particles, the particles could not be dis-

persed in water. The presence of carbon, oxygen, and silicon was confirmed *via* EDX spectroscopy, further indicating the successful polycondensation of TMVS (Fig. S3†). TMVS particles were insoluble in organic solvents and possessed a high thermal stability (T 5% = 600 °C), as confirmed *via* thermogravimetric analysis (Fig. S4†).

Since the synthesized TMVS particles were prone to sedimentation, no stable dispersion in a common solvent could be created. Therefore, structural analysis of vinylated TMVS particles was conducted utilizing scanning electron microscopy (SEM) (Fig. S5†). TMVS particles were found to be spherical in shape, resulting in a material predestined for surface-based applications due to a high surface-to-volume ratio. Particle growth over time was studied *via* SEM imaging after 0.5, 1, 2, and 4 h growing time (Fig. S6†). After an initial continuous growth, the resulting particle size of TMVS particles reached a plateau after 2–4 hours, allowing for control over the resulting particles size and therefore controlling the surface area of vinylated particles. The final diameter of vinylated particles after reacting for 4 hours was measured to be around 1.52 μm (standard deviation (SD): 0.43) (Fig. S7†). The specific surface area of TMVS particles was determined by adsorption and desorption measurements using the Brunauer–Emmett–Teller (BET) method. BET calculations revealed the specific surface area ($a_{\text{s, BET}}$) of TMVS particles to be 12.04 m^2 g^{-1} (Fig. S8†).

Vinylated TMVS particles were subjected to inverse vulcanization with elemental sulfur (Scheme 1). However, as stated by Wu *et al.*, the heteroatoms found in organo siloxane compounds deactivate the vinyl group against inverse vulcanization.[2] Thus, zinc diethyldithiocarbamate (Zn(DTC)$_2$) was employed as a catalyst during the inverse vulcanization of vinylated TMVS particles.[45] Typically, 1.0 g of vinylated TMVS particles were reacted with elemental sulfur in the presence of 100 mg Zn(DTC)$_2$ (10 wt% relative to the mass of TMVS particles) for 2 hours at 150 °C. Since sulfur acts as initiator, monomer, and solvent during inverse vulcanization reactions, an excess of elemental sulfur (around 5.0 g) was necessary in order to create a homogenous reaction mixture. Removal of excess sulfur was performed by thoroughly washing the obtained product with CS$_2$, which is known to readily dissolve elemental sulfur at room temperature.[46] In contrast to the colorless TMVS particles, the obtained inverse vulcanized product exhibited a yellow coloration, as is typical for sulfur coated silica particles (Fig. S9†).[2,35] The successful reaction of
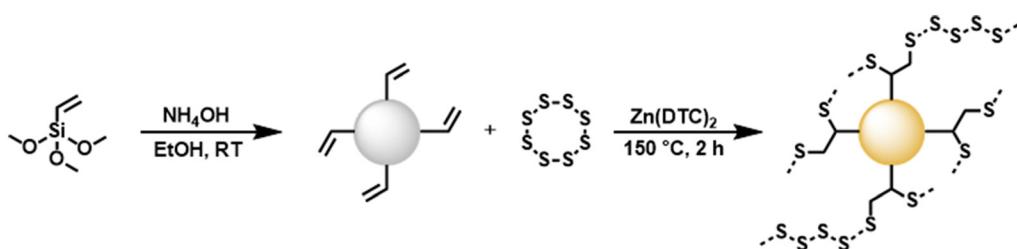
Scheme 1 Reaction equation of the inverse vulcanization of vinylated TMVS particles made by a modified Stöber method. Sulfur chains are abbreviated by dotted lines.

vinylated TMVS particles with elemental sulfur was confirmed by IR and EDX spectroscopy. Interestingly, the IR spectrum of trimethoxyvinylsilane-sulfur (TMVS-S) particles revealed no disappearance of absorbance bands attributed to vinylic C=C double bonds when compared to the IR spectrum of plain TMVS particles. Absorbance bands at 1602, 1408, and 757 cm^{-1}, characteristic for C=C$_{stretch}$, C–H$_{bend}$, and C–H$_{wag}$ vibrations in C=C–H remain pronounced in the IR spectrum of inverse vulcanized TMVS particles (Fig. 1A). This could be explained by the depth of penetration of the IR light beam into the particles during analysis which can typically be assumed at around 1–2 μm in the region of C=C double bond vibration frequencies.[47] Thus, it is believed that the presence of vinylic bond vibrations in the IR spectrum of TMVS-S particles is due to the existence of unreacted vinyl groups embedded into the particles which were not exposed to sulfur during the inverse vulcanization. However, the EDX spectrum of TMVS-S particles confirmed the presence of sulfur in the obtained material while there was no residual crystalline sulfur seen in the respective SEM image and DSC measurement (Fig. S11†). Characteristic primary K$_\alpha$ and secondary K$_\beta$ transitions were detected at X-ray energies of 2.31 and 2.46 keV respectively (Fig. 1B). It must be noted that

the appearance of zinc in the EDX spectrum of inverse vulcanized TMVS-S particles at 1.02 keV was due to the usage of Zn(DTC)$_2$ during the inverse vulcanization reaction. Previous studies on the mechanism of catalytic inverse vulcanization remain undecided regarding the remaining of the catalyst after the reaction.[2,4] However, the presence of zinc in the material after extensive washing leads us to believe that the Zn(DTC)$_2$ gets either covalently bound or trapped otherwise in the material during the inverse vulcanization, which is in line with the finding that the catalyst of inverse vulcanization reactions can generally not be regained afterwards.[2] In order to quantify the amount of sulfur coated onto the particles, elemental analysis (EA) was conducted (Table 1). It was found that the sulfur content of inverse vulcanized TMVS-S particles was as high as 18.85 wt% (SD: 0.42 wt%), which was further confirmed by thermogravimetric analysis.

The thermogram of TMVS-S particles shows a primary weight loss of around 19.6 wt% starting at around 300 °C which was attributed to the decomposition of sulfur chains during the heating process (Fig. 1C).[48] This value matched with the sulfur content previously determined by EA. SEM imaging of TMVS-S particles revealed an average increase in
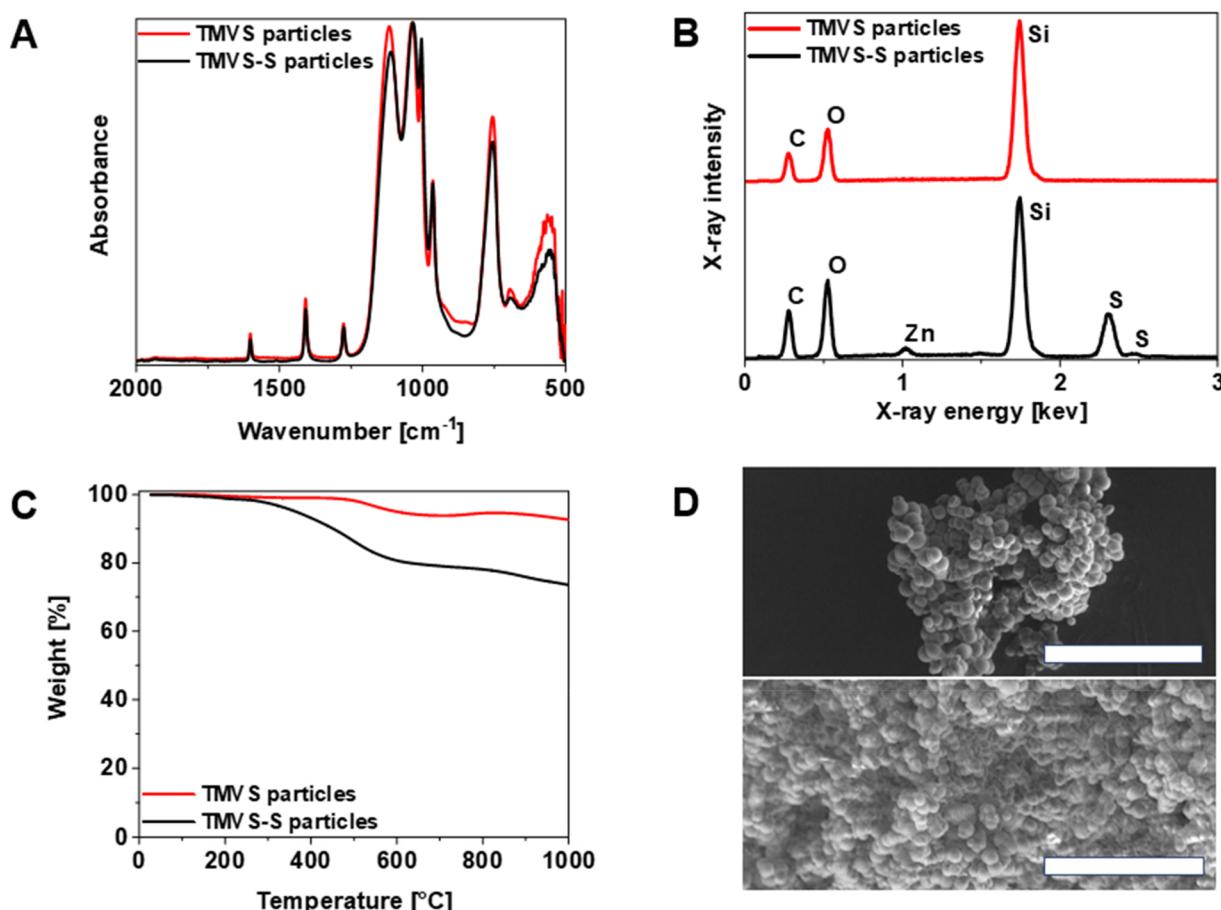

Fig. 1 Normalized ATR FT-IR (A) and normalized EDX (B) spectra of TMVS and TMVS-S particles, respectively. (C) Thermograms of TMVS and TMVS-S particles up to 1000 °C. (D) SEM image of TMVS particles (upper image) and inverse vulcanized TMVS-S particles (lower image). Scalebar is 20 μm.

Table 1 Elemental analyses of TMVS, TMVS-S, and TMVS-S-NVIA particles, respectively. SD = standard deviation

Particles	N (SD) [wt%]	C (SD) [wt%]	H (SD) [wt%]	S (SD) [wt%]
TMVS	0.00 (0.00)	25.13 (1.06)	3.99 (0.21)	0.00 (0.00)
TMVS-S	0.17 (0.01)	17.59 (1.13)	3.06 (0.07)	18.85 (0.42)
TMVS-S-NVIA	1.87 (0.01)	27.27 (2.12)	3.22 (0.02)	10.82 (0.22)

particle diameter of 0.25 μm (avg. diameter: 1.77 μm, SD: 0.36 μm) while maintaining the overall spherical geometry of particles derived from the Stöber synthesis of silica particles. The inverse vulcanization slightly reduced the specific surface area of TMVS-S particles to 11.98 m^2 g^{-1} which is in line with the observation of increasing particle size (Fig. S12†). Additionally, SEM revealed no crystalline residual sulfur among the particles, substantiating the applicability of carbon disulfide to remove excess sulfur after the inverse vulcanization of vinylated TMVS particles (Fig. 1D).[45] Inverse vulcanization of vinylated silica particles proved to be an effective method to synthesize sulfur coated silica particles with remarkable sulfur content.

Due to the dynamic nature of S–S bonds, it was reported that inverse vulcanized materials can be post-modified by dynamic covalent polymerization. This allows for simple incorporation of olefinic comonomers into high sulfur content polymers.[49] Inverse vulcanized TMVS-S particles were mixed with *N*-vinylimidazole (*N*VIA) and Zn(DTC)$_2$ and heated to 150 °C for 2 hours to obtain post-modified TMVS-S-*N*VIA particles (Scheme 2). The successful integration of *N*VIA into the sulfur chains surrounding the silica core of the particles was confirmed again by elemental analysis. It was found that the nitrogen content in TMVS-S-*N*VIA particles derived from inverse vulcanization and dynamic covalent polymerization significantly increased to 1.87 wt% when an excess of *N*VIA was employed (Table 1). Interestingly, the sulfur content of TMVS-S-*N*VIA particles decreased more than expected from 18.85 wt% to 10.82 wt%. The polysulfur previously bound in the particles is believed to have reacted as initiator to trigger both the incor-

poration of *N*VIA into the particle coating as well as the formation of the sulfur-*N*-vinylimidazole copolymer. This hypothesis is supported by the formation of a dark THF-soluble fraction during the dynamic covalent polymerization which was washed from the product after the reaction.

Consequently, we hypothesize that an equilibrium has set between sulfur-*N*VIA domains covalently coated on the silica particles, and free poly(sulfur-*random*-*N*-vinylimidazole) (poly (S-*r*-*N*VIA)) side product, which limits the incorporation of *N*VIA into the particle coating by dynamic covalent polymerization of inverse vulcanized TMVS-S particles (Scheme 2). However, the successful integration of *N*-vinylimidazole was confirmed by EDX spectroscopy with the appearance of the characteristic K$_\alpha$ transition of nitrogen at 0.39 keV (Fig. S13†). Furthermore, IR spectroscopy revealed the presence of *N*-vinylimidazole groups in the material. At 1647, 1500, and 1228 cm^{-1} the absorbance caused by ring C=C$_{stretch}$, C=N$_{stretch}$, and C–N$_{stretch}$ vibrations were identified, respectively. At around 882 cm^{-1} an absorption band associated with the ring C–H bending vibration was found. The ring torsion vibration could be assigned to a weak absorption at 654 cm^{-1} (Fig. S14†).[50] SEM imaging of TMVS-S-*N*VIA particles showed a reduction in mean particle size of around 0.20 μm (avg. diameter: 1.57 μm, SD: 0.31 μm. This finding is in line with the proposed side reaction where a significant amount of sulfur was removed from the material due to the formation of soluble poly(S-*r*-*N*VIA). Additionally, dynamic covalent polymerization of TMVS-S particles with *N*VIA yielded spherical particles with uneven and overgrown surface structure, as has been revealed by SEM (Fig. 2A) which explains the decrease in specific surface area ($a_{s, BET}$ = 11.21 m^2 g^{-1}, Fig. S15†).

It is well known that materials with high sulfur content derived from inverse vulcanization exhibit excellent remediation properties for a variety of hazardous metal ions, most notably mercury(II).[24] To demonstrate the applicability of post-modified TMVS-S-*N*VIA as adsorbent for toxic metal ions, we created aqueous solutions of mercury(II) and copper(II) chloride with different concentrations. Concentrations of both mercury(II) and copper(II) ions were set to 1000, 100, 10, and
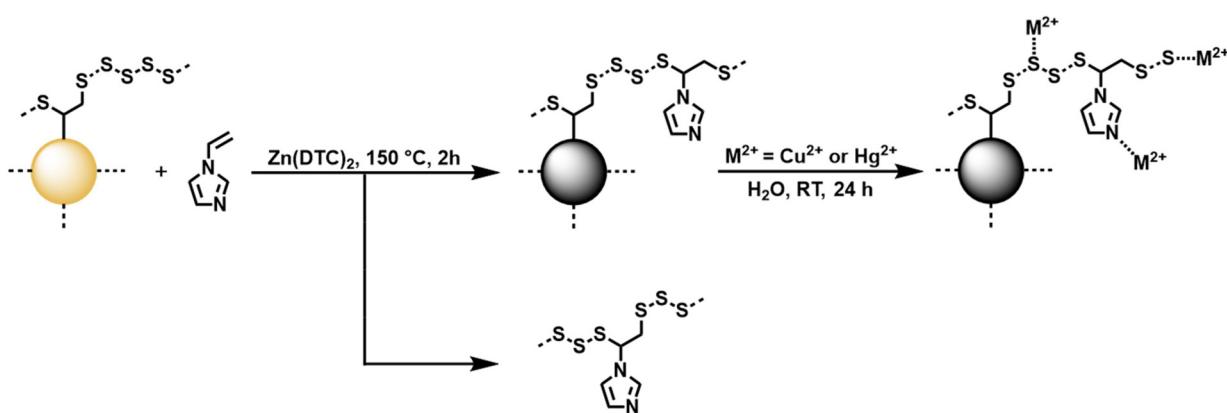
Scheme 2 Reaction equation of the dynamic covalent polymerization of inverse vulcanized TMVS-S particles with *N*-vinylimidazole to create TMVS-S-*N*VIA particles and their adsorption of Hg^{2+} and Cu^{2+} ions. Sulfur chains are abbreviated with dashed lines.
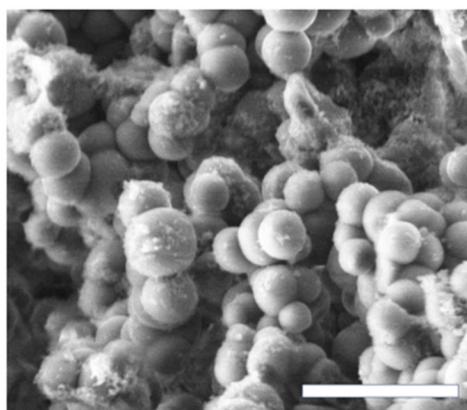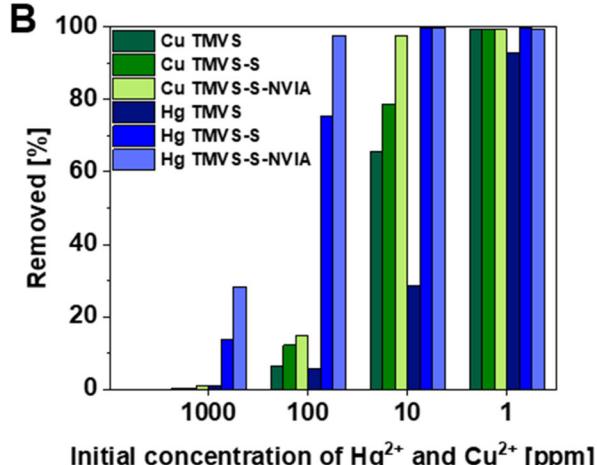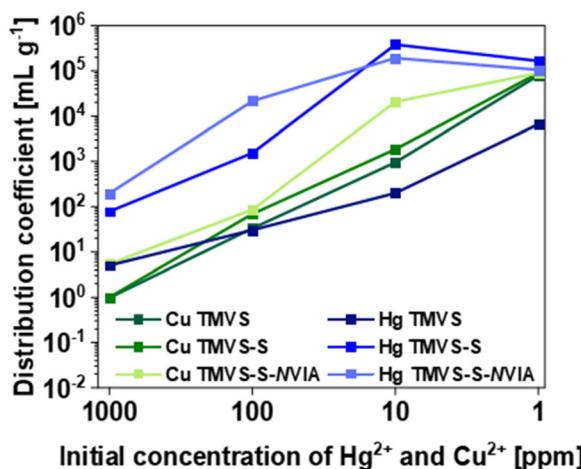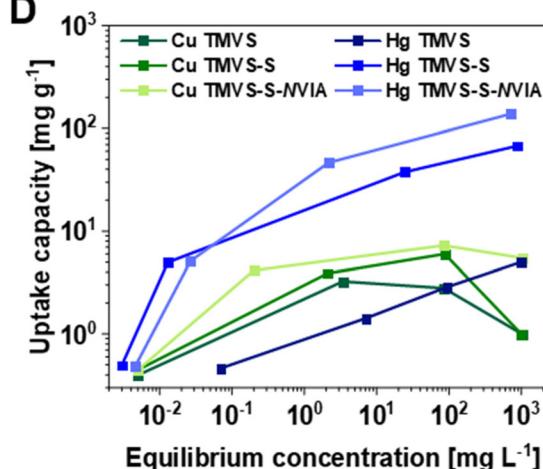
Fig. 2 (A) SEM image of TMVS-S-NVIA particles. Scalebar is 5 μm. (B) Removed copper ions (green) and mercury ions (blue) from aqueous solution by TMVS-S and TMVS-S-NVIA particles in %. Calculated distribution coefficients (C) and uptake capacities (D) of TMVS-S particles and TMVS-S-NVIA particles, respectively. Uptake capacities plotted against initial ion concentration can be found in the ESI.†

1 ppm in 100 mL deionized water. 200 mg of adsorbent were added to each solution and the mixtures were stirred for 24 hours at ambient temperature. After filtration, the resulting mercury(ɪɪ) and copper(ɪɪ) concentrations were determined by cold-vapor atom absorption spectroscopy (AAS) and inductively coupled plasma-atomic emission spectroscopy (ICP-AES), respectively. Metal removal after adsorption experiments with plain TMVS particles, unmodified TMVS-S particles, and post-modified TMVS-S-NVIA particles is displayed in Fig. 2B. Interestingly, plain TMVS particles showed a considerable adsorption performance towards copper up to an initial concentration of 10 ppm where 66% copper(ɪɪ) removal was found. This can be explained by the presence of unreacted silanol groups on the surface of TMVS particles that are known to bind copper(ɪɪ) ions from aqueous media.[51] However, the adsorption on mercury(ɪɪ) by plain TMVS particles was found to be dramatically less effective when compared to inverse vulcanized silica particles. Unmodified TMVS-S particles could remove over 99% of mercury(ɪɪ) ions up to an initial concentration of 10 ppm. Copper(ɪɪ) removal of unmodified TMVS-S

particles was found to be less effective with around 79% removal at an initial concentration of 10 ppm. The remediation of both mercury(ɪɪ) and copper(ɪɪ) ions from aqueous solutions could be significantly increased by employing post-modified TMVS-S-NVIA particle as adsorbent. At 100 ppm, mercury(ɪɪ) removal increased from 75% to 97% while the increase of copper(ɪɪ) remediation became more pronounced at 10 ppm with an increase from 79% to 98%. Interestingly, the adsorption capacity for mercury(ɪɪ) ions increased more than the adsorption capacity for copper(ɪɪ) ions at higher initial ion concentrations. This can be explained by the inherent ability of imidazole containing polymers to also effectively bind mercury(ɪɪ) ions from aqueous media.[52]

The affinity of TMVS-S and TMVS-S-NVIA particles to remove hazardous mercury(ɪɪ)- and copper(ɪɪ) ions from aqueous solutions was quantified by calculation of the distribution coefficient K_d.[53] K_d is defined as:

$$K_d = \frac{(c_i - c_f)}{c_f} \times \frac{V}{m}$$

where c_i is the initial concentration of the respective metal ion (mg L^{-1}), c_f is the concentration of the respective metal ion after the adsorption experiment (mg L^{-1}), V is the volume of the solution (mL), and m is the mass of the adsorbent (g). The distribution coefficient describes the performance of a solid sorbent for metal ion adsorption where values of 1.0×10^5 ml g^{-1} and above are considered excellent.[54] The mercury(II) and copper(II) uptake capacity Q_e of TMVS-S and TMVS-S-NVIA particles was calculated by the mass balance equation:

$$Q_e = (c_i - c_f) \times \frac{V}{m}$$

K_d and Q_e values of TMVS, TMVS-S, and TMVS-S-NVIA particles for mercury(II) and copper(II) are summarized in Tables S1–S3† and plotted in Fig. 2C and D, as well as Fig. S16.† The metal ion uptake can be attributed to the high surface area of spherical particles on the micrometer scale. The intrinsic affinity to mercury of high sulfur content materials derived from inverse vulcanization was enhanced by the ligating properties of N-vinylimidazole, which is also known to act as ligand in copper complexes.[55] Studies regarding the copper(II) adsorption of N-vinylimidazole containing polymers found a preferred coordination number of 4 for the proposed N-vinylimidazole-copper complex,[56] which indicates a similar coordination by TMVS-S-NVIA particles for the adsorption of copper(II) from aqueous media. It is believed that the increase in mercury removal observed for TMVS-S-NVIA particles compared to TMVS-S particles is caused by the additional coordination of mercury(II) by N-vinylimidazole moieties, further highlighting the applicability of N-vinylimidazole for heavy metal remediation.[57] We propose, that the tunable size of TMVS particles derived from the Stöber synthesis allows for manufacturing of efficient filter columns as industrial waste water remediation components. The intrinsic insolubility of TMVS-S-NVIA particles represents a desirable property of filter materials to not only be applicable in aqueous environments, but also in organic solvent-based systems. However, further investigations regarding the control over particle size are mandatory when designing industrial components such as filter columns to optimize the active surface area of the adsorbent by reducing the particles size. Additionally, since adsorbed heavy metal ions presumably remain in the material, periodic renewal or workup of the filter material would become necessary. Nevertheless, the underlying methodology described in this work depicts a promising route towards highly efficient filter materials for heavy metal remediation.

Conclusions

We reported the inverse vulcanization of vinylated SiO$_2$ particles with elemental sulfur. A modified Stöber synthesis was employed to create spherical vinylated microparticles derived from trimethoxyvinylsilane. Trimethoxyvinylsilane particles were subjected to catalytic inverse vulcanization which allowed the incorporation of 18.85% sulfur by weight while maintaining their spherical shape. Dynamic covalent polymerization was used as a

post-modification strategy to utilize the dynamic nature of S–S bonds and integrate N-vinylimidazole into the material. Due to the high surface-to-volume ratio of spherical microparticles, the applicability of TMVS-S-NVIA particles as adsorption material for environmentally hazardous heavy metal ions was investigated. It was found that the aromatic amine functional group of N-vinylimidazole moiety contributed very effectively in adsorbing copper(II) ions from pH neutral aqueous solutions while maintaining the inherent affinity of high sulfur content polymers to mercury. We report outstanding distribution coefficients for the adsorption of mercury(II) ions up to 100 ppm under the chosen conditions (100 mL solution, 200 mg particles). However, to gain an in depth understanding about the selectivity of TMVS-S-NVIA particles towards a broader range of hazardous heavy metal ions, further adsorption investigations with multi-ion systems are necessary, as has been done previously.[31] Nevertheless, the abundance and low cost of the compounds presented in this work make the preparation of inverse vulcanized particles a scalable approach for developing novel materials with a wide range of industrial applications, such as filters, coatings, and membranes.

Author contributions

Conflicts of interest

There are no conflicts to declare.

Acknowledgements

References

1 B. Zhang, H. Gao, P. Yan, S. Petcher and T. Hasell, *Mater. Chem. Front.*, 2020, **4**, 669–675.

2 X. Wu, J. A. Smith, S. Petcher, B. Zhang, D. J. Parker, J. M. Griffin and T. Hasell, *Nat. Commun.*, 2019, **10**, 647.

3 W. J. Chung, J. J. Griebel, E. T. Kim, H. Yoon, A. G. Simmonds, H. J. Ji, P. T. Dirlam, R. S. Glass, J. J. Wie, N. A. Nguyen, B. W. Guralnick, J. Park, A. Somogyi, P. Theato, M. E. Mackay, Y.-E. Sung, K. Char and J. Pyun, *Nat. Chem.*, 2013, **5**, 518–524.

4 L. J. Dodd, Ö. Omar, X. Wu and T. Hasell, *ACS Catal.*, 2021, **11**, 4441–4455.

5 D. A. Boyd, C. C. Baker, J. D. Myers, V. Q. Nguyen, G. A. Drake, C. C. McClain, F. H. Kung, S. R. Bowman, W. Kim and J. S. Sanghera, *Chem. Commun.*, 2016, **53**, 259–262.

6 T. S. Kleine, T. Lee, K. J. Carothers, M. O. Hamilton, L. E. Anderson, L. Ruiz Diaz, N. P. Lyons, K. R. Coasey, W. O. Parker, L. Borghi, M. E. Mackay, K. Char, R. S. Glass, D. L. Lichtenberger, R. A. Norwood and J. Pyun, *Angew. Chem., Int. Ed.*, 2019, **58**, 17656–17660.

7 T. S. Kleine, N. A. Nguyen, L. E. Anderson, S. Namnabat, E. A. LaVilla, S. A. Showghi, P. T. Dirlam, C. B. Arrington, M. S. Manchester, J. Schwiegerling, R. S. Glass, K. Char, R. A. Norwood, M. E. Mackay and J. Pyun, *ACS Macro Lett.*, 2016, **5**, 1152–1156.

8 L. E. Anderson, T. S. Kleine, Y. Zhang, D. D. Phan, S. Namnabat, E. A. LaVilla, K. M. Konopka, L. Ruiz Diaz, M. S. Manchester, J. Schwiegerling, R. S. Glass, M. E. Mackay, K. Char, R. A. Norwood and J. Pyun, *ACS Macro Lett.*, 2017, **6**, 500–504.

9 J. J. Griebel, S. Namnabat, E. T. Kim, R. Himmelhuber, D. H. Moronta, W. J. Chung, A. G. Simmonds, K.-J. Kim, J. van der Laan, N. A. Nguyen, E. L. Dereniak, M. E. Mackay, K. Char, R. S. Glass, R. A. Norwood and J. Pyun, *Adv. Mater.*, 2014, **26**, 3014–3018.

10 J. J. Griebel, G. Li, R. S. Glass, K. Char and J. Pyun, *J. Polym. Sci., Part A: Polym. Chem.*, 2015, **53**, 173–177.

11 J. A. Smith, R. Mulhall, S. Goodman, G. Fleming, H. Allison, R. Raval and T. Hasell, *ACS Omega*, 2020, **5**, 5229–5234.

12 Z. Deng, A. Hoefling, P. Théato and K. Lienkamp, *Macromol. Chem. Phys.*, 2018, **219**, 1700497.

13 S. J. Tonkin, C. T. Gibson, J. A. Campbell, D. A. Lewis, A. Karton, T. Hasell and J. M. Chalker, *Chem. Sci.*, 2020, **11**, 5537–5546.

14 Y. Xin, H. Peng, J. Xu and J. Zhang, *Adv. Funct. Mater.*, 2019, **29**, 1808989.

15 N. A. Lundquist, A. D. Tikoalu, M. J. H. Worthington, R. Shapter, S. J. Tonkin, F. Stojcevski, M. Mann, C. T. Gibson, J. R. Gascooke, A. Karton, L. C. Henderson, L. J. Esdaile and J. M. Chalker, *Chem. – Eur. J.*, 2020, **26**, 10035–10044.

16 M. Mann, J. E. Kruger, F. Andari, J. McErlean, J. R. Gascooke, J. A. Smith, M. J. H. Worthington, C. C. C. McKinley, J. A. Campbell, D. A. Lewis, T. Hasell, M. V. Perkins and J. M. Chalker, *Org. Biomol. Chem.*, 2019, **17**, 1929–1936.

17 V. S. Wadi, K. K. Jena, S. Z. Khawaja, V. M. Ranagraj and S. M. Alhassan, *RSC Adv.*, 2019, **9**, 4397–4403.

18 I. Gomez, O. Leonet, J. A. Blazquez and D. Mecerreyes, *ChemSusChem*, 2016, **9**, 3419–3425.

19 Y. Zhang, J. J. Griebel, P. T. Dirlam, N. A. Nguyen, R. S. Glass, M. E. Mackay, K. Char and J. Pyun, *J. Polym. Sci., Part A: Polym. Chem.*, 2017, **55**, 107–116.

20 A. Hoefling, Y. J. Lee and P. Theato, *Macromol. Chem. Phys.*, 2017, **218**, 1600303.

21 A. Hoefling, D. T. Nguyen, Y. J. Lee, S.-W. Song and P. Theato, *Mater. Chem. Front.*, 2017, **1**, 1818–1822.

22 A. Hoefling, D. T. Nguyen, P. Partovi-Azar, D. Sebastiani, P. Theato, S.-W. Song and Y. J. Lee, *Chem. Mater.*, 2018, **30**, 2915–2923.

23 Y. Sun, G. Zhong, Z. Zhao, M. Cao, H. Zhou, S. Zhang, H. Qian, Z. Lin, D. Lu, J. Wu and H. Chen, *Nano Lett.*, 2020, **20**, 2191–2196.

24 M. P. Crockett, A. M. Evans, M. J. H. Worthington, I. S. Albuquerque, A. D. Slattery, C. T. Gibson, J. A. Campbell, D. A. Lewis, G. J. L. Bernardes and J. M. Chalker, *Angew. Chem., Int. Ed.*, 2016, **55**, 1714–1718.

25 M. W. Thielke, L. A. Bultema, D. D. Brauer, B. Richter, M. Fischer and P. Theato, *Polymers*, 2016, **8**, 266.

26 Y. Chen, A. Yasin, Y. Zhang, X. Zan, Y. Liu and L. Zhang, *Materials*, 2020, **13**, 632.

27 V. S. Wadi, H. Mittal, E. Fosso-Kankeu, K. K. Jena and S. M. Alhassan, *Colloids Surf., A*, 2020, **606**, 125333.

28 A. D. Tikoalu, N. A. Lundquist and J. M. Chalker, *Adv. Sustainable Syst.*, 2020, **4**, 1900111.

29 B. Zhang, L. J. Dodd, P. Yan and T. Hasell, *React. Funct. Polym.*, 2021, **161**, 104865.

30 S. Akay, B. Kayan, D. Kalderis, M. Arslan, Y. Yagci and B. Kiskan, *J. Appl. Polym. Sci.*, 2017, **134**, 45306.

31 L.-A. Ko, Y.-S. Huang and Y. A. Lin, *ACS Appl. Polym. Mater.*, 2021, **3**, 3363–3372.

32 D. J. Parker, H. A. Jones, S. Petcher, L. Cervini, J. M. Griffin, R. Akhtar and T. Hasell, *J. Mater. Chem. A*, 2017, **5**, 11682–11692.

33 H. Shin, J. Kim, D. Kim, V. H. Nguyen, S. Lee, S. Han, J. Lim and K. Char, *J. Mater. Chem. A*, 2018, **6**, 23542–23549.

34 S. Petcher, B. Zhang and T. Hasell, *Chem. Commun.*, 2021, **57**, 5059.

35 J. M. Scheiger, C. Direksilp, P. Falkenstein, A. Welle, M. König-Edel, S. Heissler, J. Matysik, P. Levkin and P. Theato, *Angew. Chem., Int. Ed.*, 2020, **59**, 18639–18645.

36 J. M. Scheiger, M. Hoffmann, P. Falkenstein, Z. Wang, M. Rutschmann, V. W. Scheiger, A. Grimm, K. Urbschat, T. Sengpiel, J. Matysik, M. Wilhelm, P. A. Levkin and P. Theato, *Angew. Chem., Int. Ed.*, 2022, **61**, e202114896.

37 W. Stöber, A. Fink and E. Bohn, *J. Colloid Interface Sci.*, 1968, **26**, 62–69.

38 J. Kim, S. Park, J. E. Lee, S. M. Jin, J. H. Lee, I. S. Lee, I. Yang, J.-S. Kim, S. K. Kim, M.-H. Cho and T. Hyeon, *Angew. Chem., Int. Ed.*, 2006, **45**, 7754–7758.

39 J. Kopecek, *Biomaterials*, 2007, **28**, 5185–5192.

40 P. G. Jeelani, P. Mulay, R. Venkat and C. Ramalingam, *Silicon*, 2020, **12**, 1337–1354.

41 F. Liu, L.-X. Wen, Z.-Z. Li, W. Yu, H.-Y. Sun and J.-F. Chen, *Mater. Res. Bull.*, 2006, **41**, 2268–2275.

42 B. Kumari and D. P. Singh, *Ecol. Eng.*, 2016, **97**, 98–105.

43 E. G. Barrera, P. R. Livotto and J. H. d. Santos, *Powder Technol.*, 2016, **301**, 486–492.

44 A. Alessi, S. Agnello, G. Buscarino and F. M. Gelardi, *J. Non-Cryst. Solids*, 2013, **362**, 20–24.

45 K. W. Park, Z. Zujovic and E. M. Leitao, *Macromolecules*, 2022, **55**, 2280–2289.

46 B. Meyer, J. M. Austin and D. Jensen, *J. Chem. Eng. Data*, 1971, **16**, 364–366.

47 A. Götz, R. Nikzad-Langerodi, Y. Staedler, A. Bellaire and J. Saukel, *Spectrochim. Acta, Part A*, 2020, **224**, 117460.

48 M. Arslan, B. Kiskan, E. C. Cengiz, R. Demir-Cakan and Y. Yagci, *Eur. Polym. J.*, 2016, **80**, 70–77.

49 M. Kwon, H. Lee, S.-H. Lee, H. B. Jeon, M.-C. Oh, J. Pyun and H. Paik, *Macromol. Res.*, 2020, **28**, 1003–1009.

50 M. Talu, E. U. Demiroğlu, Ş. Yurdakul and S. Badoğlu, *Spectrochim. Acta, Part A*, 2015, **134**, 267–275.

51 A. W. Knight, A. B. Tigges and A. G. Ilgen, *Geochem. Trans.*, 2018, **19**, 13.

52 J. Sun, Z. Chen, M. Ge, L. Xu and M. Zhai, *J. Hazard. Mater.*, 2013, **244–245**, 94–101.

53 F. Ke, L.-G. Qiu, Y.-P. Yuan, F.-M. Peng, X. Jiang, A.-J. Xie, Y.-H. Shen and J.-F. Zhu, *J. Hazard. Mater.*, 2011, **196**, 36–43.

54 Y. Shin, G. E. Fryxell, W. Um, K. Parker, S. V. Mattigod and R. Skaggs, *Adv. Funct. Mater.*, 2007, **17**, 2897–2901.

55 V. I. Smirnov, L. M. Sinegovskaya, L. N. Parshina, A. V. Artem'ev and I. V. Sterkhova, *Mendeleev Commun.*, 2020, **30**, 246–248.

56 M. Takafuji, S. Ide, H. Ihara and Z. Xu, *Chem. Mater.*, 2004, **16**, 1977–1983.

57 M. J. Molina, M. R. Gmez-Antn, B. L. Rivas, H. A. Maturana and I. F. Pirola, *J. Appl. Polym. Sci.*, 2001, **79**, 1467–1475.